Electronic Supplementary Material (ESI) for Nanoscale.

Development of functional black phosphorus nanosheets with remarkable catalytic and antibacterial performance

*Qiong Wu, Meijuan Liang, Simin Zhang, Xiaoqing Liu, Fuan Wang**

Key Laboratory of Analytical Chemistry for Biology and Medicine (Ministry of Education),

College of Chemistry and Molecular Sciences, Wuhan University, Wuhan, P. R. China

* To whom correspondence should be addressed. E-mail: fuanwang@whu.edu.cn.

Table of Contents

Table S1. Quantitative analysis of Au and P elements of the as-prepared x-AuNPs/BPNs nanohybrids as determined by ICP-AES.

Samples	Au (mg/L)	P (mg/L)	Molar ratio of P/Au	Molar percentage of Au (%)	Specific surface area of AuNPs ($m^2 \cdot g^{-1}$)
23%-AuNPs/BPNs	11.00	6.05	3.50	23	36
10%-AuNPs/BPNs	14.00	18.67	8.47	10	59
5.0%-AuNPs/BPNs	14.48	43.44	19.10	5	67
2.5%-AuNPs/BPNs	13.79	86.88	40.04	2.5	107

For ICP-AES quantitative analysis, 290 μL of the respective x-AuNPs/BPNs nanohybrids were dissolved and boiled in aqua regia, followed by adding ultrapure water to a fixed volume of 10 mL.

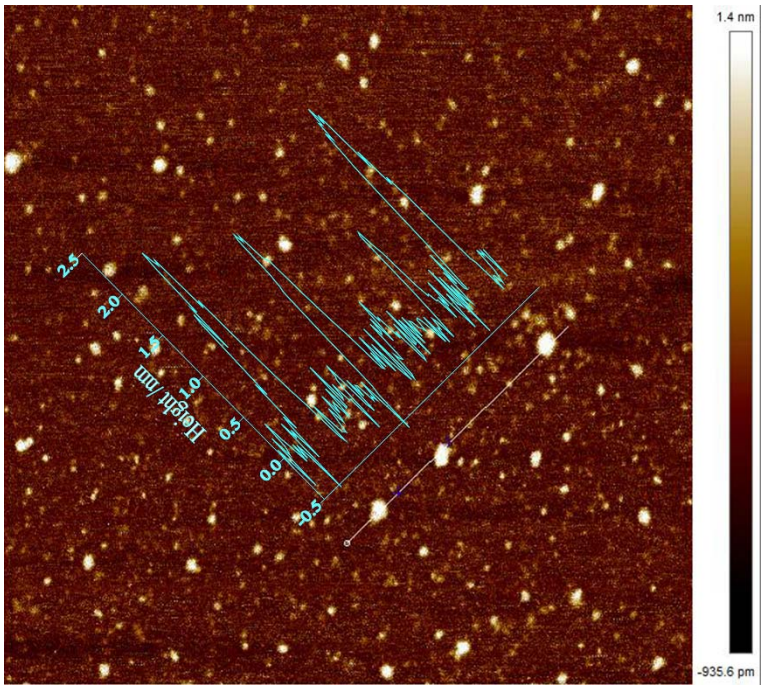

Figure S1. AFM image of exfoliated BPNs and their corresponding height analysis. An average thickness of 2 nm is acquired from the AFM measurement.

For AFM characterization of the exfoliated BPNs, a modified mica is needed by incubating the freshly cleaved mica with the gaseous mixtures of (3-aminopropyl) trimethoxysilane (APTES) and N, N-diisopropylethylamine (DIPEA) for 2 h. The BPNs sample was diluted with water and deposited on the aforementioned modified mica for 15 min to allow its adsorption, which was then washed with water and dried with nitrogen. The silicon tips used for AFM analysis were SCANASYST-AIR (tip radius: ~2 nm; resonance frequency: ~70 kHz; spring constant: ~0.4 N/m; length: 115 μm; width: 25 μm).

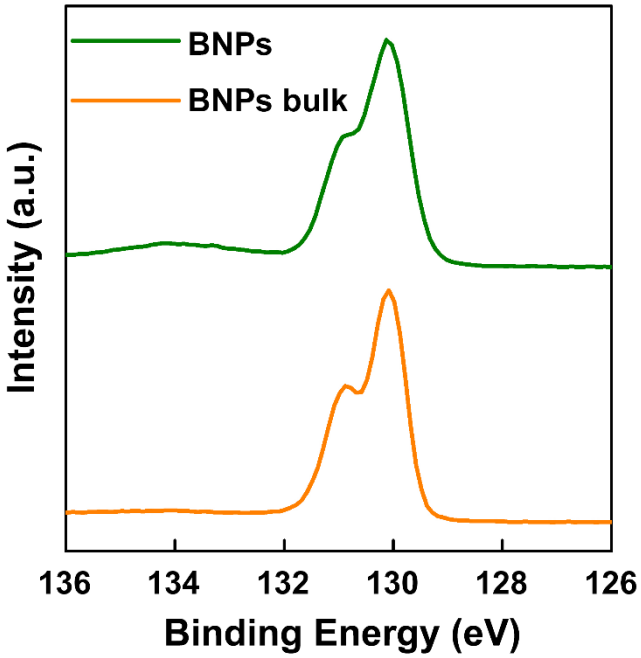

Figure S2. High-resolution XPS spectra of the P 2p for bulk BP and aqueous-exfoliated BPNs. A weakly emerged band of 133.9 eV was derived from the slightly oxidized BPNs during the aqueous exfoliation process.

For XPS characterization of the exfoliated BPNs, the silicon pellets were previously soaked in piranha solution (a mixture consisting of 7 parts of concentrated sulfuric acid and 3 parts of 30% hydrogen peroxide solution) for 2 h, and then were washed with ethanol and ultrapure water for several times. The exfoliated BPNs aqueous solution was deposited on the clean silicon pellet and dried in vacuum for subsequent XPS measurement.

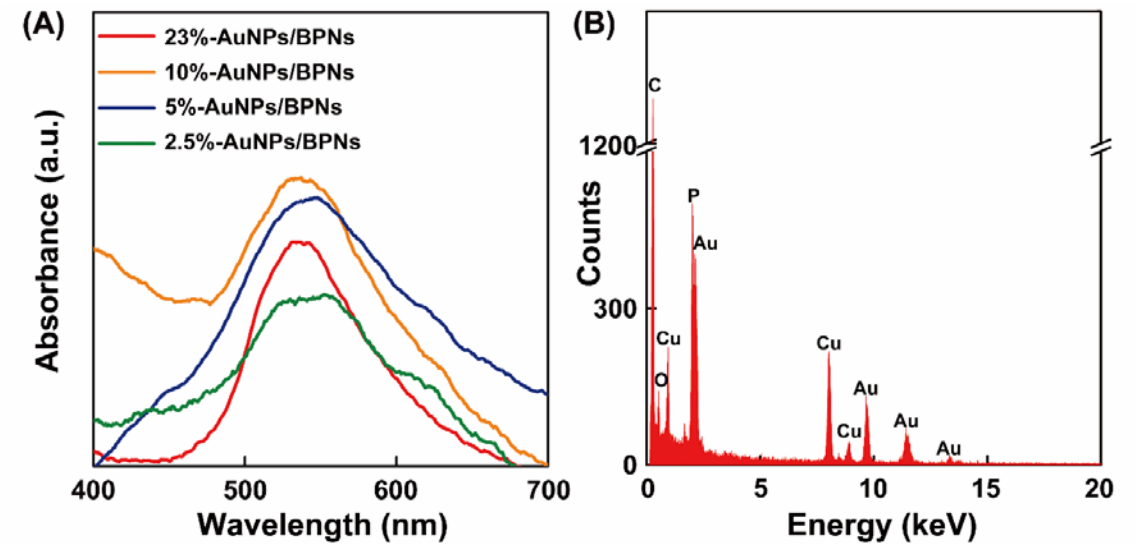

Figure S3. (A) UV-vis spectra of AuNPs derived from different x-AuNPs/BPNs nanohybrids by subtracting the absorbance of BPNs from that of nanohybrids. (B) The corresponding EDS spectrum of the typical 10%-AuNPs/BPNs nanohybrid. The EDS spectra were performed by using FEI Titan G2 electron microscope at 300 kV.

The formation of AuNPs was confirmed by subtracting the absorbance of BPNs from the corresponding hybrids. An evident derived absorption peak of ~530 nm were acquired. In this case, superficial hydrophilic suboxides of BPNs may serve as preferential reactive sites by electrostatic conjugation with $AuCl^{4-}$, followed by intrinsic reduction to produce x-AuNPs/BPNs nanohybrids. The composition of AuNPs/BPNs hybrid was acquired by EDS characterization, and characteristic peaks of O, Au and P elements (Cu and C were ascribed to the carbon grid) were observed. These results suggest that AuNPs were successfully generated by simply BPNs-assistant Au^{3+} reduction without any additional poisonous reductants or surfactants, consistent with the definition of green chemistry.

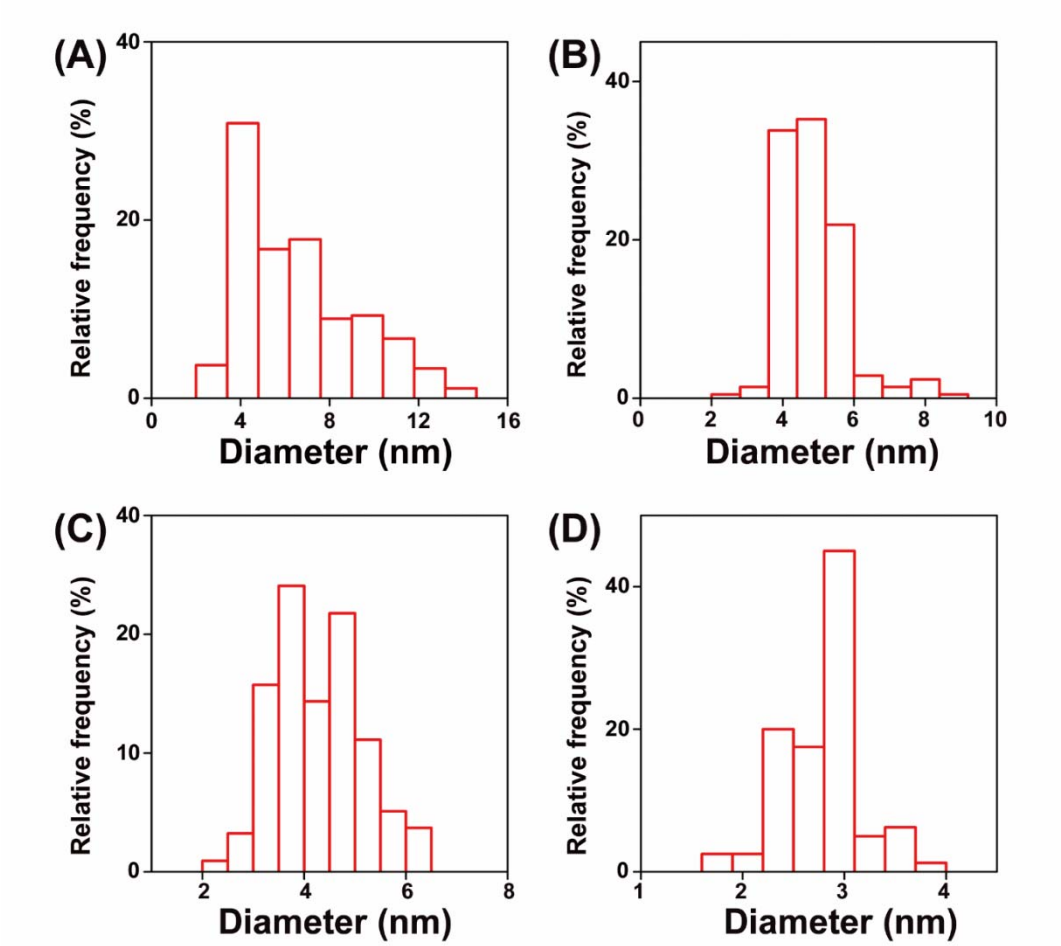

Figure S4. Size distribution histograms of AuNPs from different x-AuNPs/BPNs nanohybrids: (A) 23%-AuNPs/BPNs, (B) 10%-AuNPs/BPNs, (C) 5%-AuNPs/BPNs, and (D) 2.5%-AuNPs/BPNs. An appropriate amount of ~200 AuNPs was utilized for statistical analysis on each of the random x-AuNPs/BPNs nanohybrids.

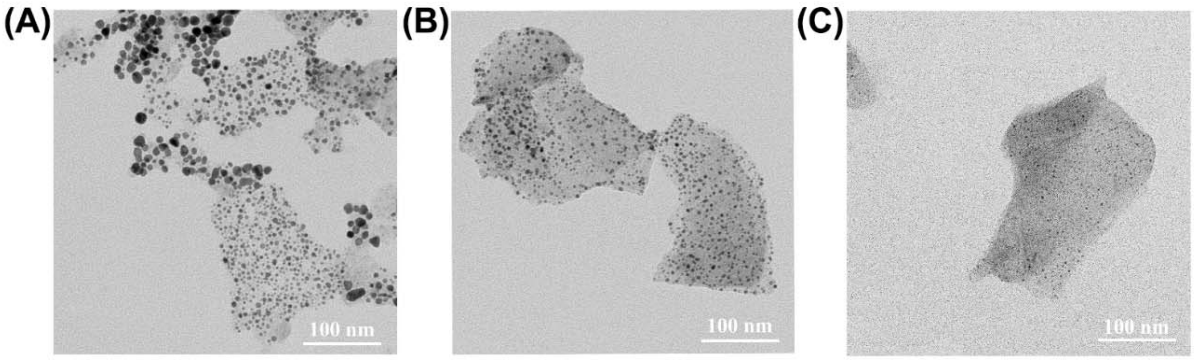

Figure S5. TEM images of (A) 23%-AuNPs/BPNs, (B) 5%-AuNPs/BPNs and (C) 2.5%-AuNPs/BPNs.

The morphological properties of x-AuNPs/BPNs nanohybrids were correlated with the BPNs-to-Au ratio. An obvious aggregated NPs with a diameter of ~10 nm was observed for 23%-AuNPs/BPNs hybrid with lower BPNs-to-Au ratio. Conversely, smaller but much lower coverage of AuNPs were deposited on the surface of BPNs for AuNPs/BPNs nanohybrids with higher BPNs-to-Au ratio (2.5%-AuNPs/BPNs and 5%-AuNPs/BPNs). It is supposed that the construction of BPNs-anchored AuNPs follows a kinetically controlled process.[1] In brief, low dosage of BPNs leads to a faster auto-reduction of Au^{3+} precursor. The relatively low coating speed of oxidized phosphorus product facilitates the growth of Au^0 species and the formation of larger AuNPs with higher surface coverage for 23%-AuNPs/BPNs nanohybrid. An increased dosage of BPNs might enhance the collision between Au^{3+} precursor and BPNs reductant, resulting in a comparable similar coating speed with that of Au^{3+} reduction. The reinforced coating effect of utmost dosage of BPNs might restrict the further growth of AuNPs and generate more Au-P binding sites, leading to a sporadic distribution of smaller-sized AuNPs for 2.5%-AuNPs/BPNs and 5%-AuNPs/BPNs nanohybrids.

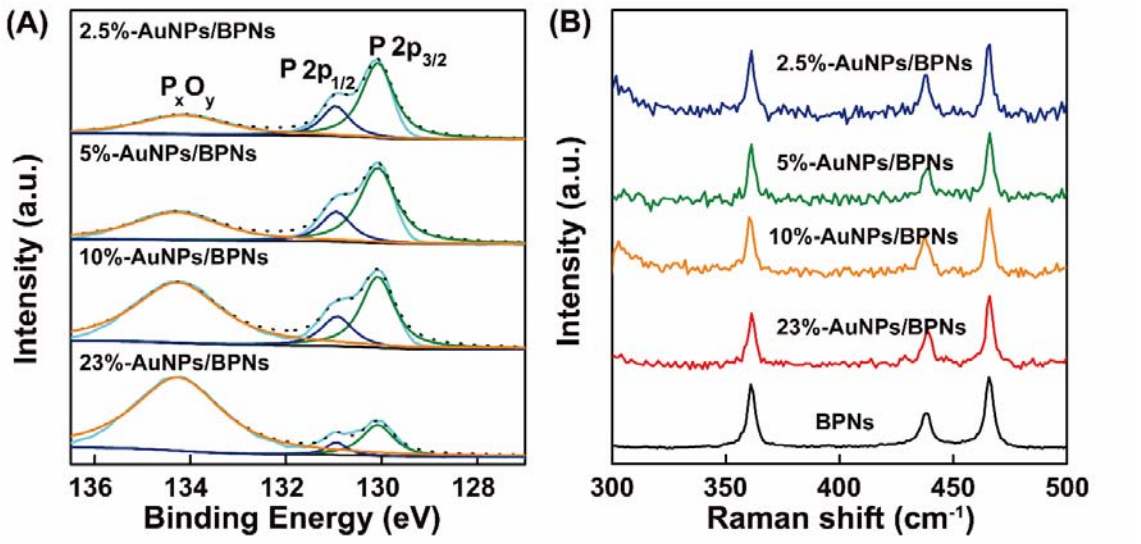

Figure S6. (A) High-resolution P 2p XPS spectra of AuNPs/BPNs nanohybrids with different molar percentage of Au. (B) Raman spectra of BPNs and x-AuNPs/BPNs nanohybrids. Dot lines represent the experimental data and solid lines show the fitted curves.

For x-AuNPs/BPNs nanohybrids, the high-resolution XPS of P band at 134.3 eV intensified with decreasing BPNs-to-Au ratio. This increased binding energy was attributed to the interaction between phosphorus oxides and surrounding Au atoms. In addition, Raman spectra of x-AuNPs/BPNs nanohybrids retained the characteristic peaks of BPNs, revealing that BPNs maintained their intrinsic structure upon $HAuCl_4$ reduction and concomitant AuNPs immobilization.

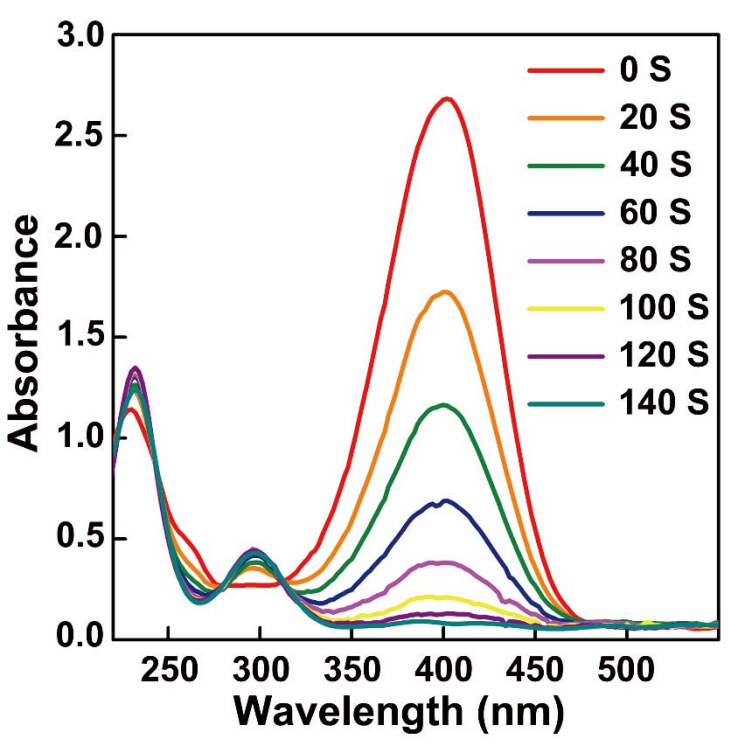

Figure S7. Typical time-dependent UV-vis spectra changes of 4-NP (λ=400 nm) upon treating the 4-NP/$NaBH_4$ mixture with 10%-AuNPs/BPNs hybrid catalysts.

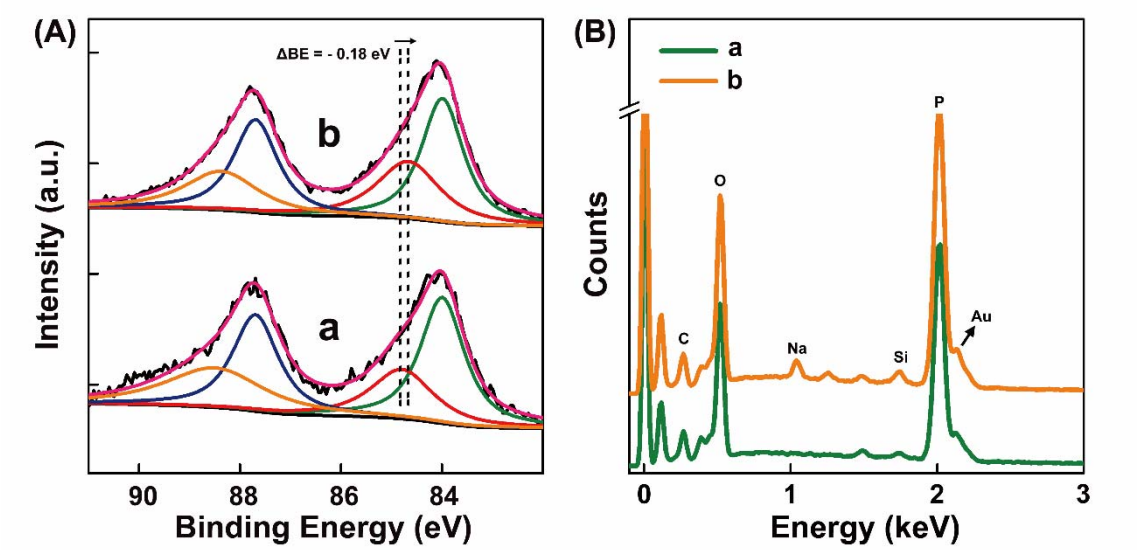

Figure S8. (A) High-resolution XPS spectra of Au 4f and (B) EDS analysis of AuNPs/BPNs (a) prior and (b) posterior to the 4-NP-involved catalysis reaction. "BE" represents "binding energy". The EDS spectra were acquired by Zeiss Merlin Compact at 30 kV.

The characteristic XPS peaks of Au^{+}-relevant species show a negative shift (-0.18 eV) after catalytic reduction for AuNPs/BPNs hybrid (**Figure S8A**). This indeed confirm that the active hydrogen species from borohydride are transferred to the surface of AuNPs that in favors of accelerating the 4-NP reduction. In addition, the AuNPs/BPNs retain their chemical components as illustrate by EDS analysis after catalytic test (**Figure S8B**). Besides, an appearance of sodium peak from the EDS spectra results from the interaction between AuNPs/BPNs and reactants.

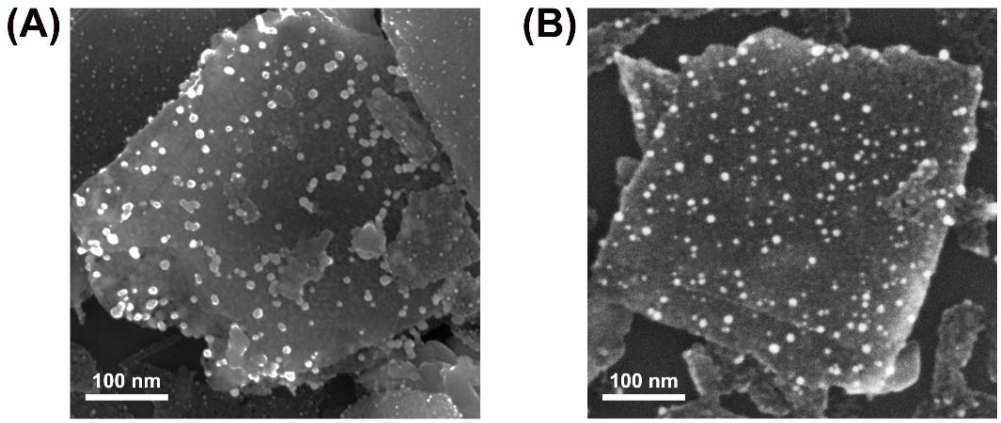

Figure S9. SEM images of AuNPs/BPNs hybrids (A) prior and (B) posterior to the 4-NP-involved catalysis reaction.

For SEM characterization, the silicon wafer were treated by immersing in piranha solution for 2 h, then were washed with ethanol and ultrapure water for several times. The AuNPs/BPNs-involved catalytic solutions were centrifuged and the resulting AuNPs/BPNs precipitate was washed and re-suspended in water, dropped onto the silicon wafer and dried in vacuum for acquiring SEM images. Clearly, BPNs-supported AuNPs retained their intact morphological features after catalytic reactions, demonstrating the robustness of the present AuNPs/BPNs nanohybrids. Here the BPNs accommodates appropriately AuNPs and prevents AuNPs from aggregation and passivation, resulting in a synergistic enhancement effect between BPNs and AuNPs for sustainable efficient catalysis processes.

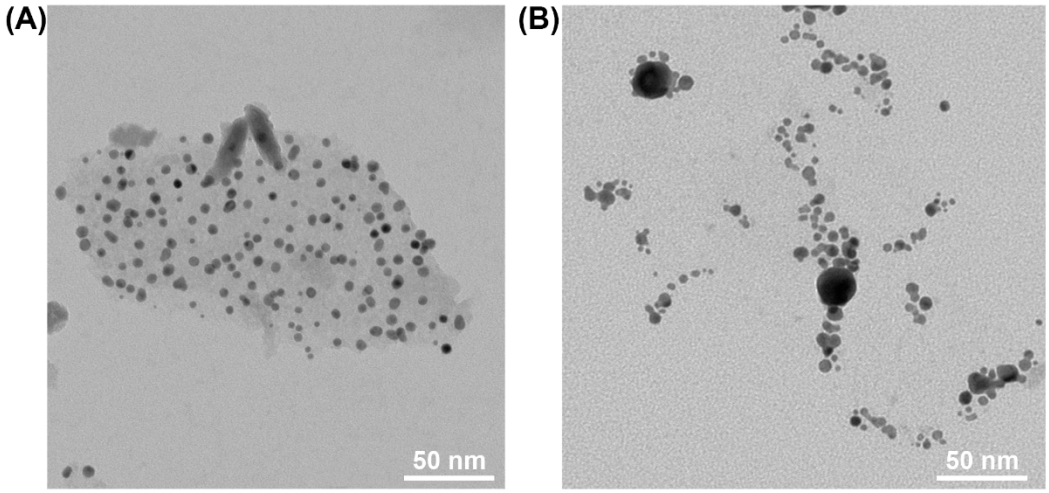

Figure S10. TEM image of 10%-AuNPs/BPNs nanohybrids (A) and AuNPs (B) collected from 6 successive cycles of catalytic reactions.

To verify the stabilities of AuNPs/BPNs nanohybrids and AuNPs after repeated catalytic tests, TEM was applied to characterize the hybrids and AuNPs collected from 6-round of successive catalytic reactions. The AuNPs/BPNs hybrids and AuNPs were respectively introduced into $NaBH_4$ (60 mM, 2.62 mL) and 4-NP solution (2 mM, 300 μL) for catalytic reaction. After each round of reaction, the nanohybrids were separated by centrifugation and were introduced into the next round of reaction mixture containing newly prepared $NaBH_4$ and 4-NP solutions. The as-synthesized BPNs/ AuNPs hybrids retain their intact morphological features (**Figure S10A**) while the bare AuNPs are prone to aggregate and grow into larger nanoparticles (**Figure S10B**), demonstrating the indispensable role of BPNs for reliable and sustainable catalysis applications.

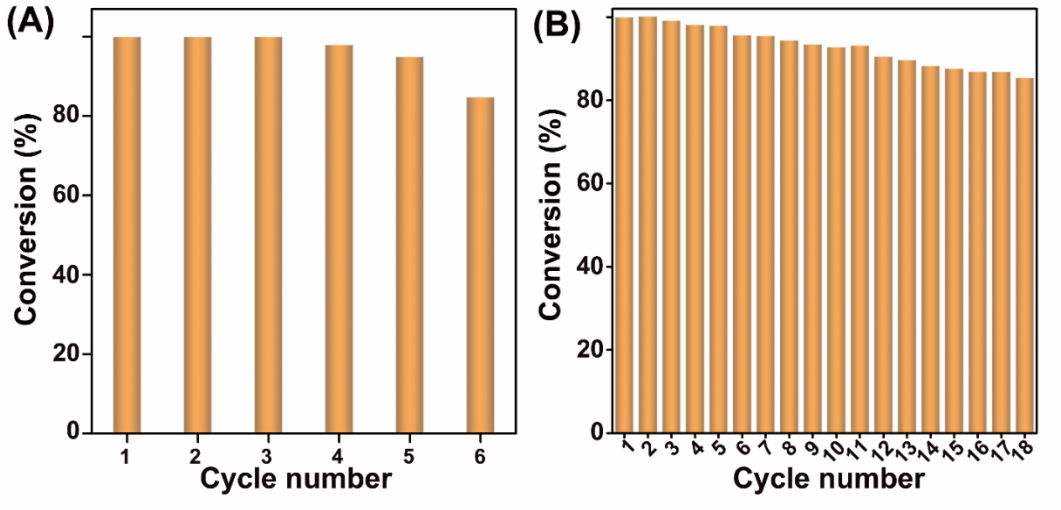

Figure S11. (A) Reusability of the 10%-AuNPs/BPNs catalyst for $NaBH_4$-mediated reduction of 4-NP in successive six cycles of experiments. (B) Conversion of 4-NP in 18 successive reaction cycles with 10%-AuNPs/BPNs nanohybrids.

We challenged the reusability of the AuNPs/BPNs nanohybrids (**Figure S11A**). The catalyst was collected and recycled by a simple centrifugation method for the subsequent round of catalytic reaction. A satisfactory catalyst-mediated 84.5% conversion within 120 s was acquired after six rounds of centrifugation and collection, demonstrating the high reusability of the catalyst. In addition, the catalyst was demonstrated to have an excellent stability, as revealed by the superior 85.2% conversion within 120 s after 18 successive cycles of catalytic reaction by using 10%-AuNPs/BPNs nanohybrid as an example. Briefly, after each catalytic reaction, another 4-NP solution (2 mM, 300 μL) and $NaBH_4$ (60 mM, 2.62 mL) were successively introduced into the reaction solution for 18 times (**Figure S11B**). These results definitely confirmed the high stabilities and robustness of the as-prepared AuNPs/BPNs nanocatalysts, which showed great potential in future practical applications.

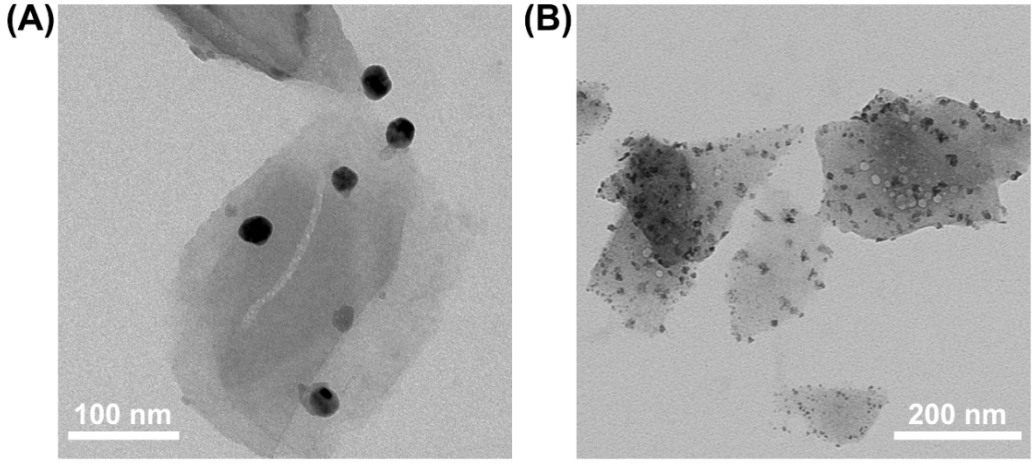

Figure S12. TEM images of highly dispersed (A) AgNPs/BPNs and (B) MnO_2/BPNs nanohybrids.

The synthesis procedure of fabricating AgNPs/BPNs hybrids is similar to that of AuNPs/BPNs nanohybrids. The BPNs dispersion was ultrasonicated, and then was introduced with $AgNO_3$ aqueous solution dropwisely and mixed slightly. AgNPs/BPNs hybrids were thus obtained by incubating the $AgNO_3$/BPNs mixture at room temperature overnight. Similarly, after adjusting the pH of BPNs solution to 10-11 with NaOH, $KMnO_4$ solution was added slowly under severely stirring to achieve the MnO_2/BPNs nanohybrids.

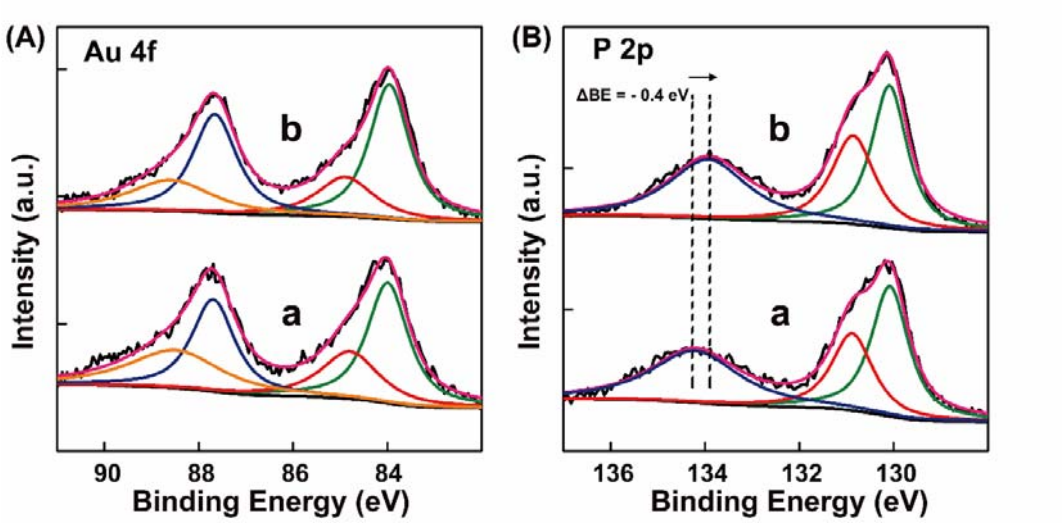

Figure S13. High-resolution XPS spectra of (A) Au 4f and (B) P 2p of AuNPs/BPNs (a) prior and (b) posterior to the antibacterial experiment. Black line is original data and other lines are fitting curves.

The percentage of Au^0 increases from 58.61% to 65.48% (percentage of $Au^0 = S_{Au^0} / (S_{Au^+} + S_{Au^0})$, S_{Au^0} and S_{Au^+} indicate respectively the corresponding fitting peak area of Au^0 and Au^+, **Figure S13A**) and the binding energy of phosphorus oxide decreases from 134.3 to 133.9 eV after the antibacterial experiments for AuNPs/BPNs hybrids (**Figure S13B**), revealing that both of AuNPs and BPNs can interact and target *E.coil*, as the bacteria can mediate the reduction of high valence Au species to low valent Au species and a concomitant electron transfer to BPNs.[2] The electron transfer of bacteria might participate in the present antibacterial procedure, as electron transfer on bacteria can influence their viability.[3]

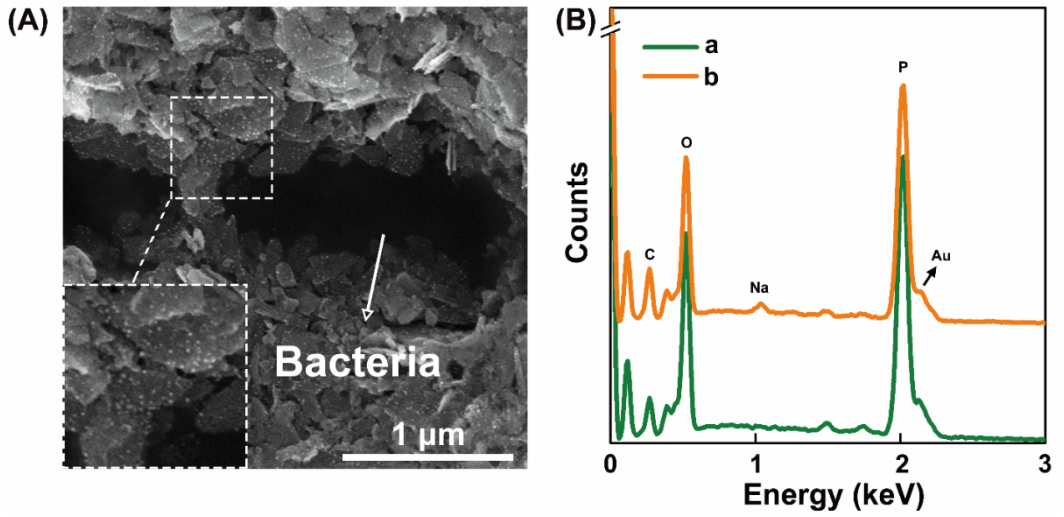

Figure S14. (A) SEM image of AuNPs/BPNs after the antibacterial experiment. (B) EDS analysis of AuNPs/BPNs (a) prior and (b) posterior to the antibacterial experiment. The EDS spectra were acquired by Zeiss Merlin Compact operated at 30 kV.

From the SEM image (**Figure S14A**) and EDS analysis (**Figure S14B**), the AuNPs/BPNs retain their intact morphological structures and chemical compositions, which is attributed to the appropriate BPNs accommodation and the accompanying high stability of AuNPs. This ensures the highly efficient and sustainable antibacterial performance of AuNPs/BPNs hybrids.

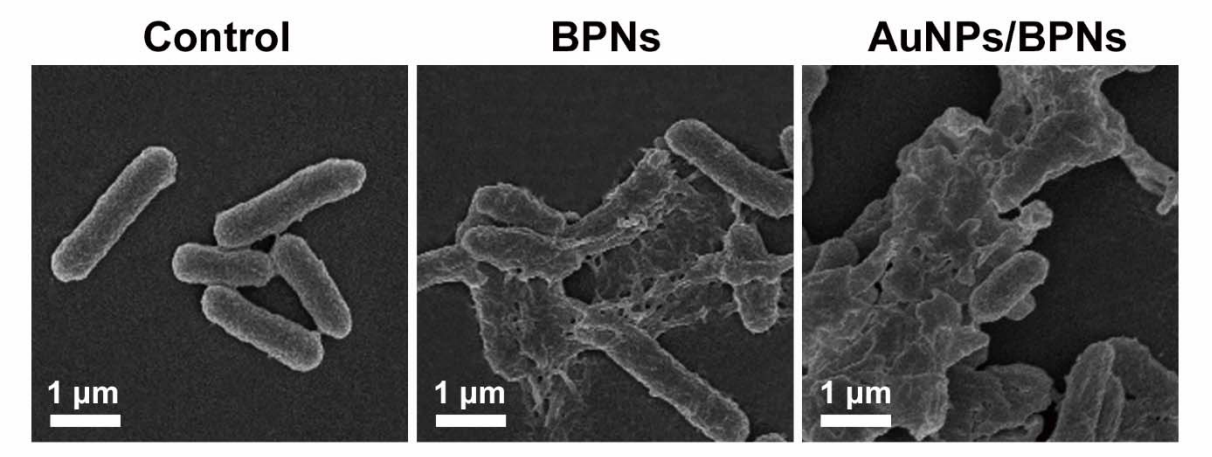

Figure S15. SEM images of *E.coil*. after incubation with ultrapure water (control), BPNs (P: 3.6 μg) and AuNPs/BPNs (P: 3.6 μg, Au: 2.7 μg).

The morphological features of intact and treated *E.coil.* were characterized by SEM. The bacterial suspensions were incubated with BPNs and AuNPs/BPNs for 8 h at 37 °C. After centrifugation at 6000 rpm, the condensed bacteria were fixed with 2.5% glutaraldehyde, post-fixed with 1% aqueous OsO_4 and washed with 0.1 M, pH 7.0 phosphate buffers. Then, the samples were consecutively dehydrated in an ascending ethanol series (30, 50, 70, 80, 90 and 100%) for 15 min. Finally, the treated bacteria suspensions were dropped on silica wafer and dried in a vacuum oven for further SEM observation. Obviously, the intact and smooth cell surfaces of rod-shaped *E.coil*. are wrinkled and broken upon its incubating with BPNs or AuNPs/BPNs hybrids (**Figure S15**).

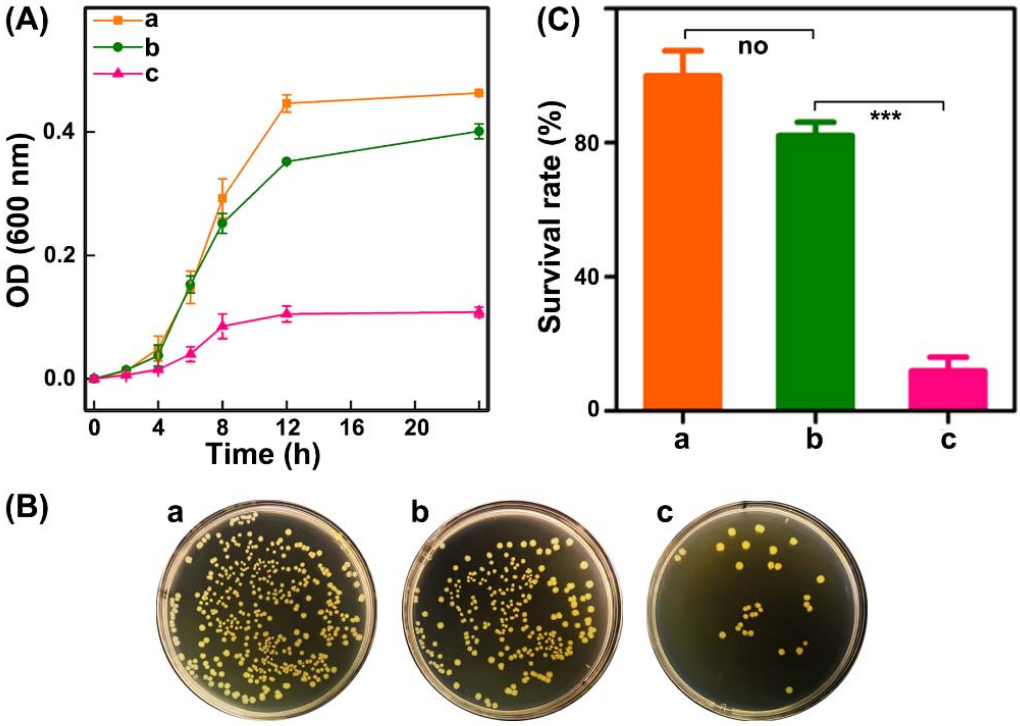

Figure S16. (A) Growth curves, (B) LB-agar plate images and (C) the corresponding surviving rate of *E.coil.* upon its exposure to (a) water, (b) AuNPs/C_3N_4 (the synthesized method is referred to a previously reported work[4]) and (c) AuNPs/BPNs with the same dosage of Au element (Au: 2.7 μg, BPNs or C_3N_4: 3.6 μg). Statistical significance was calculated using Student's t-test between AuNPs/C_3N_4 and AuNPs/BPNs or control group. "***" indicates $p < 0.0005$, "no" indicates no statistical significance ($p = 0.1035$).

It is clear that AuNPs/BPNs hybrids show a much higher antibacterial activity than that of AuNPs/C_3N_4 hybrids without an auxiliary H_2O_2 assistance (**Figure S16**). Although AuNPs/C_3N_4 hybrids exhibit high antibacterial activity in the presence of an additional H_2O_2 exposure. However, this auxiliary H_2O_2 reagent might bring undesired cytotoxicity and delay of wound healing. The unique features of our AuNPs/BPNs nanohybrids can also be revealed by their convenient and highly-efficient antibacterial operation without any extraneous agents, and also their ultimate innocuous degrading products.

References

1. H. Wu, X. Huang, M. Gao, X. Liao; B. Shi, *Green Chem*. 2011, **13**, 651-658.
2. L. W. Du, H. Jiang, X. Liu and E. Wang, *Electrochem. Commun.*, 2007, **9**, 1165-1170.
3. G. Wang, W. Jin, A. M. Qasim, A. Gao, X. Peng, W. Li, H. Feng and P. K. Chu, *Biomaterials*, 2017, **124**, 25-34.
4. Z. Wang, K. Dong, Z. Liu, Y. Zhang, Z. Chen, H. Sun, J. Ren and X. Qu, *Biomaterials*, 2017, **113**, 145-157.